INNOVATIVE SOLUTION FOR LARGE LNG COMPRESSION TRAINS USING 2-POLE INDUCTION HELPER MOTOR FED BY VOLTAGE SOURCE INVERTER

Lionel Durantay, PhD
Chief Technology Leader
GE Power Conversion
Champigneulles, France

Ty Clark
Electrical Engineer
Dominion Energy
Glen Allen, Virginia, USA.

John Paschal
Chief Engineer Electrical
Kiewit Engineering Group Inc.
Houston, Texas, USA

Niccolò Spolveri
Electrical Lead Engineer
Baker Hughes GE
Florence, Italy

Lionel Roth
Lead Technical Project Manager
GE Power Conversion
Champigneulles, France

Pierre-Paul Vivier
Senior Technical Sales Staff Manager
GE Power Conversion
Houston, Texas, USA

Lionel Durantay graduated from the ENSEM (Ecole Nationale Supérieure d'Electricité et de Mécanique) with an engineering degree in 1989 then passed PhD in 1993. He has developed innovative variable speed motors and generators solutions for Oil and Gas and Renewable businesses, including 100,000hp VFD-driven synchronous motors. He has authored or coauthored 35+ technical papers. He presently holds 12+ patents. He is currently Chief Technology Leader in GE's rotating machines group. lionel.durantay@ge.com

Ty Clark earned his B.S. in electrical engineering in 2003 from the General Motors Institute. Upon graduation, he joined ACRA Control as an application engineer, where he oversaw the development and implementation of aerospace telemetry systems. In 2008, he joined Dominion Energy as an Electrical Engineer, where he has supported the design and construction of major capital projects. He has coauthored 2 technical papers. ty.clark@dominionenergy.com

John Paschal, P.E., is the Chief Electrical Engineer for Kiewit Engineering Group, Inc. He was the Owner's Engineer for the world's largest electrically-driven LNG plant featuring nine 100,000hp VFD-driven motors and compressors. John has been the Lead Electrical engineer on several LNG plants worldwide. He has authored twenty electrical engineering books and 18 technical journal articles. john.paschal@kiewit.com

Niccolò Spolveri is currently working as Lead Electrical System Design Engineer at GE Oil & Gas in Florence, Italy. He joined GE O&G in 2012 as Lead Electrical System Engineer and he is responsible for the integration of Variable Speed Drive System for complex projects mainly for LNG applications up to 100,000hp. He got master's degree in Electric Engineering at University of Bologna, Italy in 2009. niccolo.spolveri@bhge.com

Lionel Roth graduated from the ENIM (Ecole Nationale des Ingénieurs de Metz) in Mechanical Engineering, in 2006. He led several induction and synchronous motors customization fed by VSDS for Oil & Gas Business, including 100,000hp VFD-driven 2-pole synchronous motors. He has coauthored 2 technical papers. He is currently Lead Technical Project Manager in GE's rotating machines group. lionel.roth@ge.com

Pierre-Paul Vivier graduated from the ESME Sudria in Electrical Engineering, in 2005. He joined Converteam Group in 2012 as Power Electronic Technical leader dedicated to Oil & Gas project. He led Indian engineering antenna in Chennai. He is currently Senior Technical Sales manager for North America in GE's system group, involved for complex electric LNG projects of VFD-motor systems up to 100,000hp.
pierre-paul.vivier@ge.com

ABSTRACT

This paper reviews the selected global architecture of an 85MW LNG compression train featuring a 2-pole 20MW DFE-VSI induction motor starter-helper system for a plant in the US. The first part of this paper presents the comparison between the synchronous motor powered by a load switching inverter (LCI) and the induction motor powered by a voltage source inverter (VSI) for the simplification of the electric lineup and the elimination of inter-harmonics. The simple Reliability Availability Maintainability (RAM) analysis of these two electric systems is also summarized. An innovative 10kV Neutral-Point Piloted (NPP) topology for the valves of the inverter is described. The second part of this paper focuses on the motor operating 5MW above the current power limit for 2-pole induction motors and describes the good design practices and the power limitation of the squirrel cage rotor technology. The final section is dedicated to the electrical system and the validation tests at full speed and full load. It presents the results of motor factory acceptance tests compliant to API 541, string tests, and train commissioning, thereby validating the system performance.

1. INTRODUCTION

Electric variable speed helpers used in combination with gas or steam turbines to drive large compressors have well-known advantages, including reduced downtime and accurate speed control, and are independent of ambient temperature. Large Load Commutated Inverter (LCI) systems utilizing 2-pole synchronous machines are a proven and widely implemented approach for the helper system in LNG train applications. Nevertheless, the LCI absorbs reactive power from both the grid and synchronous motor when commutating thyristors, and an LCI solution generates current harmonics that flow back into the grid. These current harmonics may result in reduced grid stability and can interact with source impedance to create voltage distortion, both of which are tightly controlled by IEEE 519. Additionally, inter-harmonics on the load side of the LCI drive may induce main air-gap torque pulsations from the motor. Keeping in mind that the accidental loss of a helper motor is extremely intrusive to the process and that a false trip can amount in production losses, it makes sense to improve the robustness and the reliability of the helper system. Generally, synchronous motors are employed for power levels greater than 15 MW even if synchronous motors are less reliable than induction motors. The system efficiency is improved by 1 to 2% when using a 2-pole motor, eliminating the gearbox. An alternative and innovative system solution consists of combining the most powerful gearbox-less 2-pole induction motor in the world with a Neutral-Point Piloted (NPP) Voltage Source Inverter (VSI) that provides advantages in plant foot-print reduction, grid integration, simplification of the electromechanical arrangement, and reduced electro-mechanical interactions with the shaft line, improving significantly the system reliability.

2. SYSTEM ARCHITECTURE AND DRIVE

A. Starter Helper Compression Train Architecture

The selected global architecture is an 85MW LNG compression train featuring a 2-pole 20MW motor starter-helper system. The configuration of the gas turbine with three compressors and an electric motor is chosen because it can accommodate all the services (mixed refrigerant and propane) on the same shaft for a single liquefaction train [1]. Being copied, the liquefaction plant has a parallel train configuration, allowing 365 days of production including maintenance of one driver. The helper motor is designed to compensate for the gas turbine's lack of power during the hottest days, allowing full production during the year. A helper is also used as a starter, reducing the gas flared during startup.

Based on a 13.8kV grid configuration, the optimum system is combining the step transformer, the drive and the motor, maximizing the return of investment and the availability. Only two parameters must be considered as key drivers (figure 1):
- The voltage $\overline{V}$ defining the transformer, the drive and the stator of the motor.
- The speed (or rotor pulsation) ω_r imposed by the choice of the gas turbine at 3600 rpm defining the rotor of the motor, in a gearless solution.

B. Conventional Electric Solution

The traditional solution consists of LCI drives (Load Commutated Inverter) has been used for more than 30 years because higher ratings of thyristors have been available (figure 3). As the thyristors need the reactive power coming from the motor to commutate, this technology can only be used with synchronous motors [2]. The LCI requires reactive power on its both sides to commutate its thyristors. On the motor side the required reactive power is provided by the motor. Therefore, LCIs can only be used with synchronous motors. This type of converter generates harmonic currents of order of the stator frequency f_s as follows:

$$k * 6.f_s \pm 1 \quad \text{where k is an integer } \{1, 2, 3...\} \tag{1}$$

These harmonic currents are the source of torque harmonics that are applied to the motor-compressor shaft line. For large powers, a typical configuration is to use a double winding synchronous motor, with a 30° phase shift between them. Each winding is fed by a 6 pulse thyristors inverter, thus providing a 12-pulse arrangement. In that configuration, the generated torque pulsations are at a $k*12f_s$ order. In the same way, this type of converter generates on the grid harmonic currents of order of the grid frequency f_g as follows:

$$k * 6.f_g \pm 1 \quad \text{where k is an integer } \{1, 2, 3...\} \tag{2}$$

To comply with the grid codes, these harmonic currents must be reduced by means of harmonic filters connected to the network. To reduce the size of those harmonic filters, a 12-pulse configuration is also generally used on the grid side as shown on the Fig 1. The design of harmonic filters can become quite challenging when the LNG trains power is increased. The LCI type of converter generates also inter-harmonic currents whose frequency is the result of a combination of the frequencies and their multiple frequencies of the supplying network and of the fundamental frequency of the motor (depending on its rotating speed). For a 12-pulse configuration on both supply and motor side, the inter-harmonic currents are the combination of:

$$| (k*12)* f_g \pm (k'*12)* f_s | \quad \text{where k and k' are integers} \tag{3}$$

These inter-harmonic currents generate pulsating torques that can create a Sub Synchronous Torsional Interaction (SSTI) [3]. Torsional interaction occurs when the induced sub synchronous torque in the motor is close to one of the torsional natural modes of the motor-compressor shaft (represented by the red dotted lines on the Campbell diagram on Figure 2).
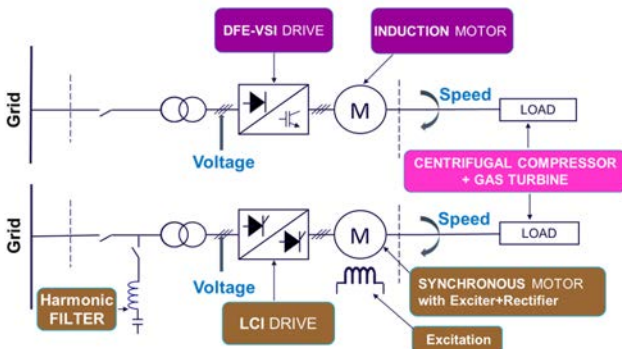

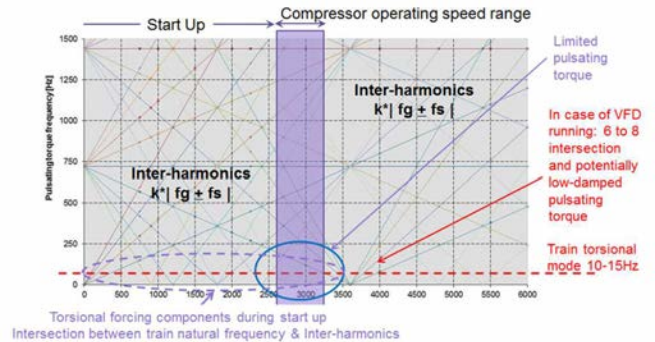**Figure 1 - Architectures of Electric Compression**

Figure 2 - Campbell Diagram for a 2 Poles Motor Fed by a 12 Pulse LCI
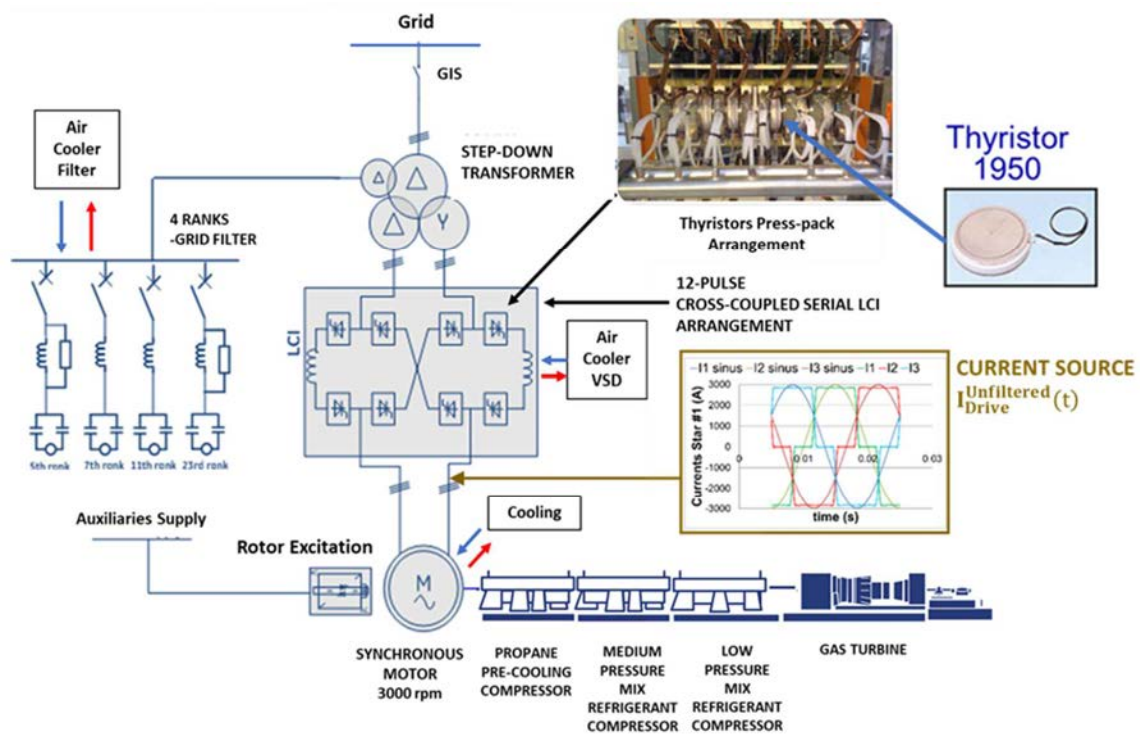
Figure 3 - Overview of a Large LCI one Line Diagram for Starter Helper Compression Train

C. Innovative Electric Solution

Replacing LCI, Pulse Width Modulated (PWM) Voltage Source Inverter (VSI) driven medium and high voltage machines up to 15kV are seen the fastest growth in various industrial applications because of their flexibility in speed control, high efficiency, high compactness, variable power factor controls compatible to synchronous or induction motor configuration. The VSI technology with various topologies using insulated-gate bipolar transistor (IGBT) devices are now gradually transitioned to Injection Enhanced Gate Transistor (IEGT) press pack devices for higher power capabilities (figure 4). All those new switching devices are operating at very high frequency of commutation. Fast switching (high dV/dt) voltages with high repetitive frequencies from these drives can degrade electrical insulation systems at much faster rate than the traditional sine waved voltages. To address this problem, practical approaches are [4] [5]:

- to increase insulation, build to sustain higher electrical stress. IEC60034-18-42 has assigned to evaluate and qualify insulation in rotating machines fed by the inverter.
- to add RLC filters (Sinus filter) in the inverter output to reduce the dV/dt of pulsed voltages lower than 3kV/µs and to prevent failure due to cables resonance.

The high power PWM VSI drive inverter is available for more than 10 years in a 3-level topology with the Neutral Point Clamped by diodes. With such a topology and thanks to the large capacity of the power devices, a VSI inverter composed of a single power device per arm can deliver around 15 MVA with an output voltage of 3.3 to 3.6 kV. In a refinement of the diode-clamped converter, the so-called Neutral-Point Clamped (NPP) converter, the clamping diode valves are replaced by IEGT ones giving additional controllability. Each valve is commutating with only half the DC bus voltage, reducing the devices commutation losses by three. With the same topology and the same power devices with the same current capability, the output power can naturally be increased by stacking in series many devices in each valve. The output voltage is thus increased proportionally to the number of power switches per valve, each device being operated with the same current and sharing the same voltage.

An innovative 10kV Neutral-Point Piloted (NPP) topology for the valves of the inverter downsizes the cooling unit of the drive. The vertical valves are composed of 6 IEGTs that are connected in series and the horizontal ones (the clamping ones) are composed of 2 valves of 4 IEGTs in a head to tail connection. Such an inverter delivers 32 MW with an output voltage of 10 kV. The technology is derived from the LCI one and all the ancillary components are embedded in the stack. The Front End of a VSI is connected to the supplying grid. Its role is to produce the pseudo constant DC voltage that will be chopped by the inverter to deliver the adequate voltage and frequency to the motor. The Diode Front End (DFE) is composed of one or more diode GRAETZ bridges, usually connected in series. As the current cannot be reversed in the diodes, its usage is restricted to drives that do not require power regeneration from the

motor to the grid to brake the driven load. It is suitable for VSIs driving centrifugal compressors. Like the LCI rectifier bridges, the DFE rectifier bridges generate harmonic currents of order $k*6f_g\pm1$. To avoid harmonic filters and thanks to the modest cost of the diodes, DFE are usually composed of multiple bridges to reduce the low ranks harmonic currents. For large drives, the coefficient k is then set to high values, as high as 6 or even 8 to meet the IEEE519 requirements. The figure 16 shows on the VSI of this application with a 36 pulses DFE (k = 6). The harmonic currents generated are at the 35th rank and above, with less than 8% of current Total Demand Distortion (TDD) as requested by the IEEE519.

Compared to LCI converter, it presents the simplification of the electrical lineup and details the elimination of the large reactive power compensators (capacitors) and of the harmonic filters and explains the simplification of the motor overcurrent protection. The decoupling between the rectifier and the inverter is much higher in a VSI than in LCI. The DC energy stored in the VSI DC capacitors is by far greater than the one stored in the LCI DC reactors. This is the main reason why VSIs do not produce significant voltage torque ripple inter-harmonics at low frequencies. As the VSI inverter generates voltage harmonics V_h to the motor (by opposition to the LCI inverter that generates current harmonics I_h) the higher the motor impedance Z_h is, the lower the harmonic currents are ($I_h = V_h / Z_h$). The design of the motor can thus be freely done so that the short-circuit torque is reduced.
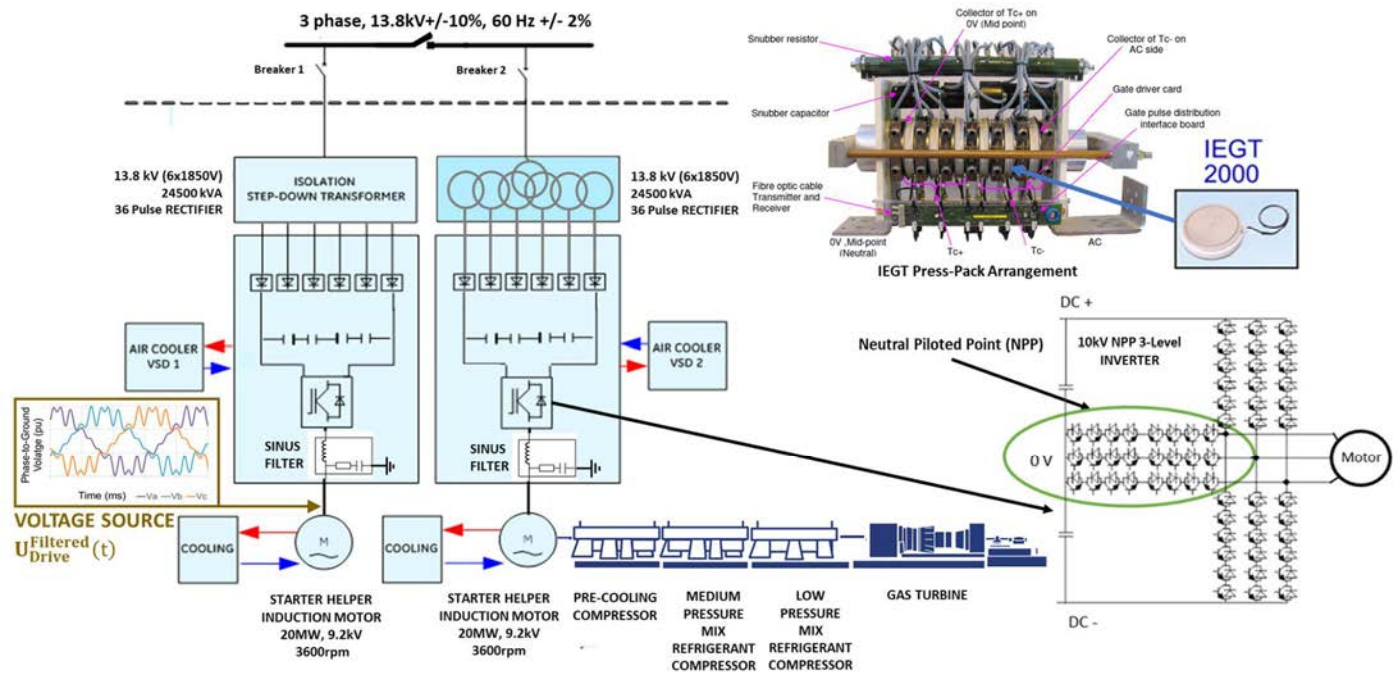

Figure 4 - Overview of a Large 10kV NPP 3-Level VSI one Line Diagram for Two Starter Helper Compression Trains

D. RAM and Electric System Solutions Pros & Cons

Another very important factor is the reliability and the availability of the equipment since any stop of the compressors may lead to high production losses. The squirrel cage rotor is maintenance-free, and the stator is well designed and protected by the sinus filter. The RAM analysis (table 1) is based on an operating fleet of more than 130 high speed induction motors operating up to 7MW@15000 rpm and 250 2-pole synchronous motors and generators up to 120MW@3600rpm over a 30-year period. The MTBF (Mean Time Before Failure) considered in this analysis is the time before the first failure, without any maintenance of the system. The Life Time of the two systems is more than 25 years. According to IEC 60034-1, the induction rotor is robust and is qualified up to 180°C in continuous service duty (type S1) and up to 200°C in transient conditions of loads [2] [6].

Table 1 – RAM {LCI 2-Pole Synchronous Motor} vs {VSI 2-Pole Induction Motor}

Parameters	Units	LCI / 2-pole Synchronous	NPP VSI / 2-pole induction
DRIVE MTBF	Years	5.5	6.0
MOTOR MTBF	Years	8	13
DRIVE MTTR	Hours	40	8
Availability	% per year	99.85%	99.92%

The following "Pros & Cons" comparison highlights the advantages of the VSI system (table 3) versus the LCI one for synchronous machines (table 2) in term of CAPEX and OPEX with a better reliability and operability [2]:

Table 2 – LCI Synchronous Motor System Pros & Cons

PROS	Lot of references up to 75MW
CONS	Weak network stability and utilities integration
CONS	Large harmonics pollution to the grid
CONS	Critical torque harmonics on shaft line
CONS	Required external harmonics filter
CONS	Motor Layout and Weight oversizing at leading PF=0.9 needed for the LCI thryristors commutations
CONS	Large static and transient loads oversizing foundations

Table 3 - VSI Induction Motor System Pros & Cons

PROS	Improved network stability and grid integration
PROS	Low harmonics content, external filter not required
PROS	Reduced torque ripple at shaft level
PROS	No risk of torsional vibration
PROS	Simpler rotor technology w/o excitation system
PROS	Better Capex Better Opex (+0.5% of Efficiency Improvement)
PROS	Low static & transient loads downsizing foundations
PROS	Less rotor natural frequencies interactions because no exciter
PROS	Increased motor + drive system availability (+0.07%)
CONS	2-pole Induction new references up to 20 MW

3. MOTOR

The three-phase synchronous motor was invented first by Friedrich August Haselwander in 1887. The three-phase squirrel-cage-rotor induction motor was invented first by Mikhail Dolivo-Dobrovolsky in 1889, only two years later. Over the time, those two technologies have been improved to withstand high peripheral speed with 2-pole machines operating up to 3600 rpm for direct-on-line configuration and possibly above 3600 rpm for variable speed applications, including the induction shaftless machine [6] and permanent magnet synchronous machine for very high-speed conditions [7].

A. Conventional Solution

As the LCI thyristors need the reactive power coming from the motor to commutate, this technology can only be used with the synchronous motor operating at leading 0.9 Power Factor impacting the size and the weight of the motor [2]. The rotor is supplied with DC current into insulated coils fed by a rectifier exciter device and creates a rotor magnetic field which follows the stator rotating field (figure 6). The exciter stator carries the exciter AC primary winding which is fed from an auxiliary VSD. The exciter rectifier diodes are one of the neuralgic components in terms of reliability. In the case of a 3-phase conventional rectifier bridge, the conduction failure of a diode causes a short circuit of the bridge and the system shutdown. The rotor shaft and body are machined from a single forging shaft. The field winding incorporates direct cooling of the copper wires and is fitted into slots in the rotor body. Alloyed copper wedges and retaining rings secure respectively the coils in the slots and the end-windings. The maximum peripheral speed with this technology is around 200 m/s limited by the mechanical stresses inside the wedges and the retaining rings.

The exciter with the rectifier is usually built as a cantilever on the opposite side of the coupling for easy access in case of diode replacement. This complicates the mechanical design of the shaft line because the critical mode of bending of the exciter can interact with mechanical excitations under variable speed conditions (figure 5).
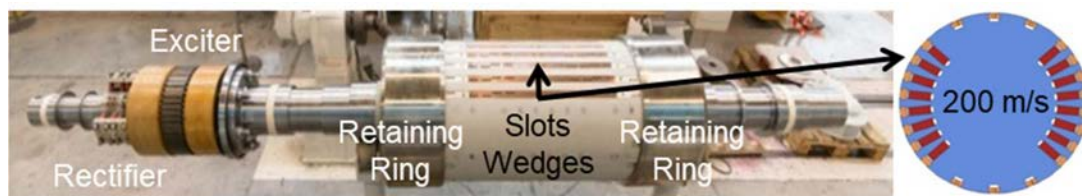

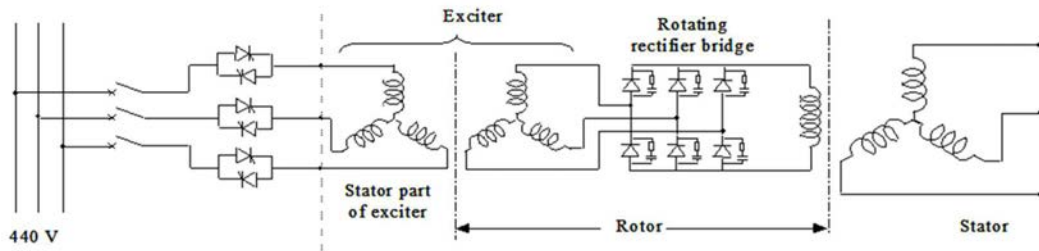**Figure 5 - Solid 2-Pole Synchronous Rotor Technology**

Figure 6 - Synchronous Motor Electric Circuit

B. Induction Solution

    a. Induction Motor Construction

In an induction motor, the three stator windings create a rotating magnetic field. Its frequency of rotation is called the synchronism frequency. The rotor consists of copper bars not insulated, short-circuited at their end by two conductive rings and constitute a "squirrel cage" (figure 8). The cage is swept by the rotating magnetic field. When a resistant torque ($\vec{\Gamma}_{load}$) is applied on the shaft by the load, it induces a rotor slippage (Ω_{rs}) with a rotor pulsation (Ω_r) a bit lower than the stator pulsation (ω_s/p) which is fixed by the control of the inverter (figure 7):

$$\Omega_{rs} = (\omega_s/p) - \Omega_r \tag{4}$$

The slip (sl) is equal to:

$$sl = \Omega_{rs}/\omega_s \tag{5}$$

The Lorentz Force induces the rotor current into the cage:

$$\vec{I}_r = \kappa_1 . q . \overrightarrow{\Omega_{rs}} \wedge \vec{B}_s \quad \text{where } \kappa_1 \text{ is a coefficient} \tag{6}$$

If the rotor turns at the same frequency as the stator field, then no torque is produced. As the rotor speed decreases with respect to the stator electric frequency ("slip") torque is produced. The Laplace Force induces the torque generation in opposite to the resistant (load) torque:

$$\vec{\Gamma} = \vec{F} . R_{Rotor}^{Outer} = \left(\kappa_2 . \vec{I}_r \wedge \vec{B}_s\right) . R_{Rotor}^{Outer} \quad \text{where } \kappa_2 \text{ is a coefficient} \tag{7}$$
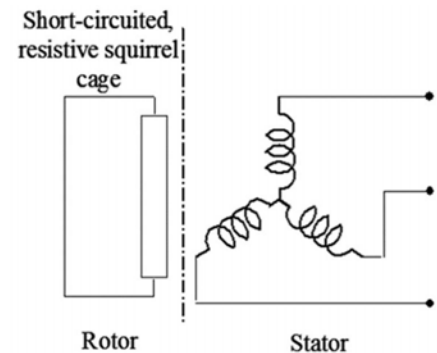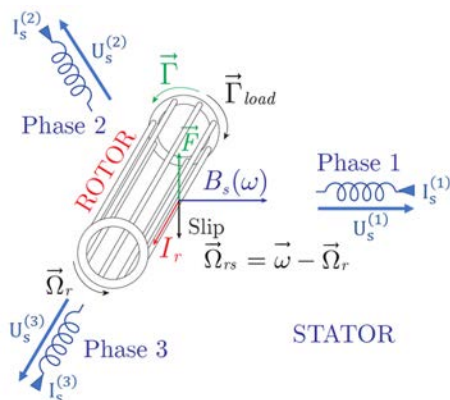
Figure 7 - Principle of Torque Generation in a Squirrel Cage Induction Motor   **Figure 8 - Induction Motor Electric Circuit**

The main components of an induction motor are the same than the synchronous motor. The stator is made of laminations and coils which are Vacuum Pressure Impregnated with Class-H Resin (figure 10) and the bearing technology being 4-lobe sleeves with oil forced hydrodynamic lubrication (figure 12), except the rotor which is a squirrel cage. The advantages of the induction motor compared to the synchronous motor include no excitation system and simplified rotor construction, leading to longer run-time with fewer maintenance issues (figure 11). The cooling with motor-fans is chosen for a better operability especially at low speed using the electric motor for the compressor and gas turbine barring (figure 13).

Figure 9 – Rotor Manufacturing

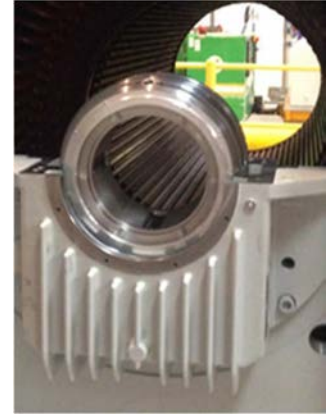**Figure 10 - VPI Stator**

Figure 11 – Assembly

Figure 12 – 4-lobe bearing

This technology has been used in the past up to 15MW. The main motor innovation is the rotor construction, customized for conditions of high centrifugal stresses, especially the squirrel cage and the laminated ferromagnetic part hooped on the shaft achieving powers now in the range of 26MW to 3600 rpm. These studies are presented later in this paper. The construction of the rotor is simple with only 15 components compared to the synchronous ones having more than 150 parts (figure 14).
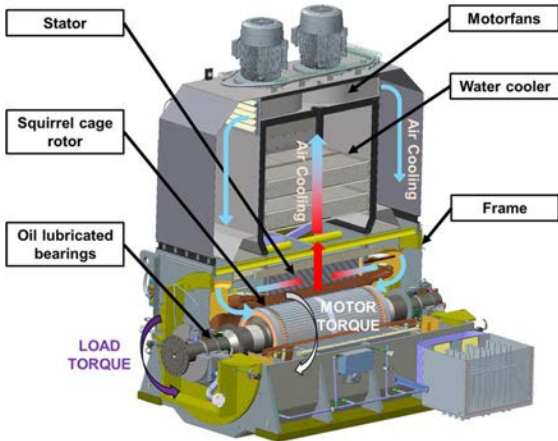
Figure 13 - Motor Thermal Cooling
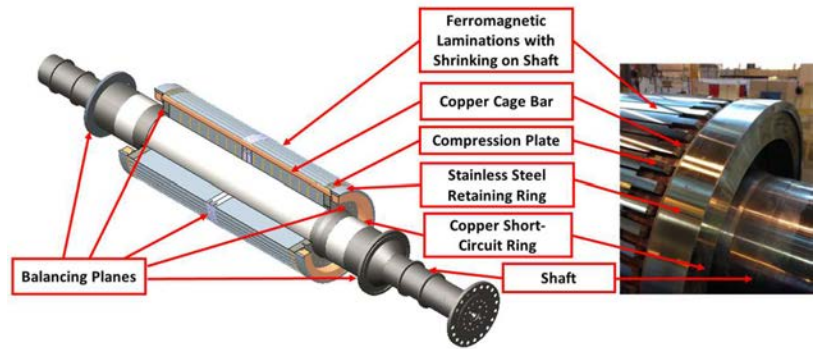
Figure 14 - Laminated Ferromagnetic Part Hooped on Shaft Arrangement

   b.   Motor Electromechanical Integration

    The vector control of squirrel cage machine was developed in the 1980s and is known and robust (Figure 15). It utilizes vector detection of the position of the rotor without speed sensor, to maximize output torque. The use of analytical electromechanical and thermal models is usually enough to predict the behavior of direct on line (DOL) machines. However, electromagnetic advanced numerical models are needed for a variable speed design considering the drive interaction with the synchronous motor. A Finite Element 2D transient model is used (figure 16). It accounts for the motion analysis (rotor slippage) and the non-linear permeability of ferromagnetic materials, incorporating all spatial (from motor) and time harmonics (from filtered drive) at a defined load. The formulation by magnetic potential vector **A** helps in reducing the time of calculation and the memory consumption of the computer. The filtered voltage from the drive $\mathbf{U_{Drive}^{Filtered}}(t)$ is directly injected into the model which calculates the induction field (Fig. 22), the losses and the stator currents with a high level of accuracy (Fig.23):

   Magnetic Potential Vector **A**: $\mathbf{B} = \text{curl } \mathbf{A}$ (8)

$$\mathbf{curl}\,(1/\mu\,\mathbf{curl\,A}) + \frac{1}{\rho}\left(\frac{\partial \mathbf{A}}{\partial t} + \boldsymbol{\nabla}\,V\right) = \mathbf{J} + \mathbf{J_s}(\mathbf{U_{Drive}^{Filtered}}(t)) \tag{9}$$
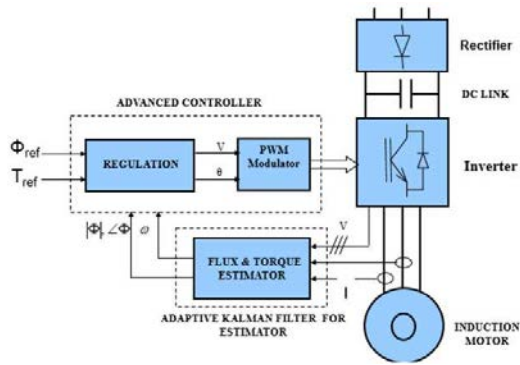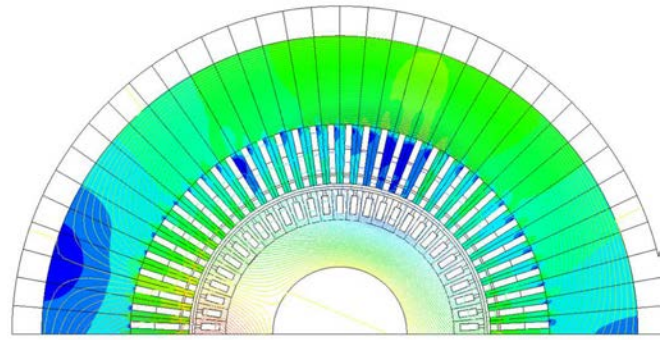
Figure 15 - Torque Control of Induction Motor

Figure 16 - 2D Finite Element Induction Field

The magnetic induction in the airgap of the motor is calculated including the time and space harmonics coming from respectively the drive interaction and the effect of reluctance in between the rotor slots and stator slots interaction. The Maxwell Tensor $[T_m]$ is used to calculate the electromagnetic torque pulsation $\Gamma(t)$ applied on both sides of the airgap, on the rotor and the stator:

$$F = \int_s [T_m].n \, dS = \int_S (\sigma_n.\vec{n} + +\sigma_t.\vec{t}) \, dS \quad \text{where} \quad \sigma_n = \frac{B_n^2 - B_t^2}{2\mu_0} \; ; \; \sigma_t = \frac{B_n.B_t}{\mu_0} \; ; \; \mu_0 = 4\pi.10^{-7} \tag{10}$$

$$\Gamma = F \wedge R_{Rotor}^{Outer} \quad \text{where } R_{Rotor}^{Outer} \text{ is the rotor radius} \tag{11}$$

The pole passing frequency excitation F_{pole} on the stator bore diameter at twice motor frequency ($2xf_s$) is given as follow for a $2p=2$ pole motor (Fig.19):

$$F_{pole} = \iint_S \sigma_n(\theta)dS \quad \text{where } B_n(\theta)=B_n.\cos(p\theta) \quad \text{and} \quad p=1 \tag{12}$$

$$F_{pole} = \frac{B_n^2 \, l \, R_{Stator}^{Inner}}{2 \, \mu_0} \int_{-\pi/2}^{\pi/2} \cos2\theta \, d\theta = \frac{\pi \, B_n^2 \, l \, R_{Stator}^{Inner}}{4 \, \mu_0} \quad \text{where } R_{Stator}^{Inner} \text{ is the stator inner radius} \tag{13}$$

As the VSI inverter generates voltage harmonics V_h to the motor (figure 17) (by opposition to the LCI inverter that generates current harmonics I_h) the higher the motor impedance Z_h is, the lower the harmonic currents are $I_h = V_h / Z_h$ (figure 18). The design of the motor can thus be freely done so that the short-circuit torque is reduced. Because of the 5 pulses control of the inverter, the harmonics of the torque proportional to the product $I * V$ to are mainly driven the 6th rank at 360 Hz and the 18th rank at 1080 Hz respectively around 3% and 7% of the mean torque remaining low (figure 20), far above the first shaft-line's torsional natural frequencies (figure 28). There is no risk of torsional vibrations coming from the electric motor compared to a motor fed by LCI with inter-harmonics around 60Hz.
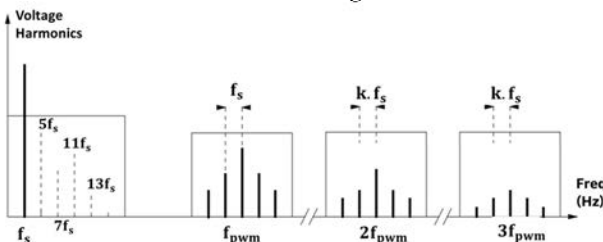

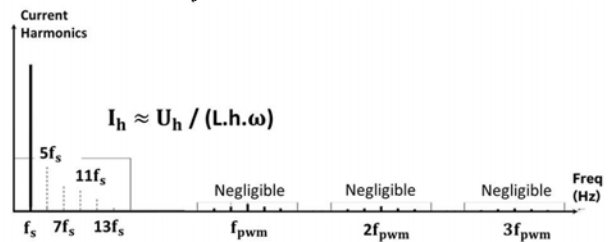**Figure 17 – Typical PWM Voltage Spectrum Pattern**

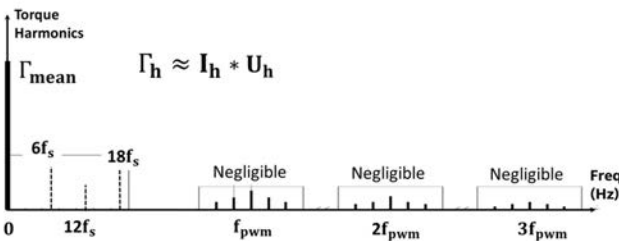**Figure 18 – Typical PWM Current Spectrum Pattern**

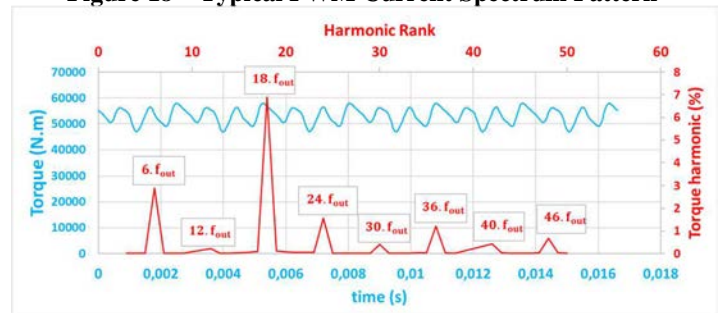**Figure 19 – Typical PWM Torque Spectrum Pattern**

Figure 20 – PWM Torque Harmonics Calculation

c. *Rotor electromechanical optimization*

The most critical point of design is securing the electromechanical dimensioning of the ferromagnetic laminations of the rotor. On one hand, the shrinking of lamination inducing hoop stress must be dimensioned without exceeding the elastic limit of the material, so as not to disconnect the laminations to the shaft when operating at overspeed condition due to the static centrifugal effects of centrifugation (figure 21). On the other hand, the design of the rotor tooth geometry should avoid any risk of coincidence of the eigenfrequencies of the teeth (figure 22) with the electrodynamic excitations arising from the reluctance interactions of space harmonics between the rotor and stator teeth. These dynamic stresses are superimposed on the static hooping and centrifugal stresses, the point of the most critical stress concentration being the bottom edge of the slot.

The large 4-pole variable speed motors are the most sensitive to these risks of resonances that can cause the cracking of the rotor teeth by a mechanism of high cycle fatigue, having induction levels in the air gap around 0.9 to 1 Tesla and air-gaps less than 10mm. In addition, the value of the bending mode of the tooth is generally around 1 to 3 kHz by sizing the cross-section of the squirrel cage bars, which corresponds to the stator excitation frequencies of the 4-pole motor in large variable speed range conditions [8]. The 2-pole motors are less sensitive having inductions around 0.7 to 0.8 Tesla and air-gap greater than 10mm decreasing a lot the effects of electrodynamic excitation. Our design rules are clearly to avoid exciting the eigenfrequencies of teeth with rank 1 linear coincidences and rank 2 parametric excitations (figure 23).
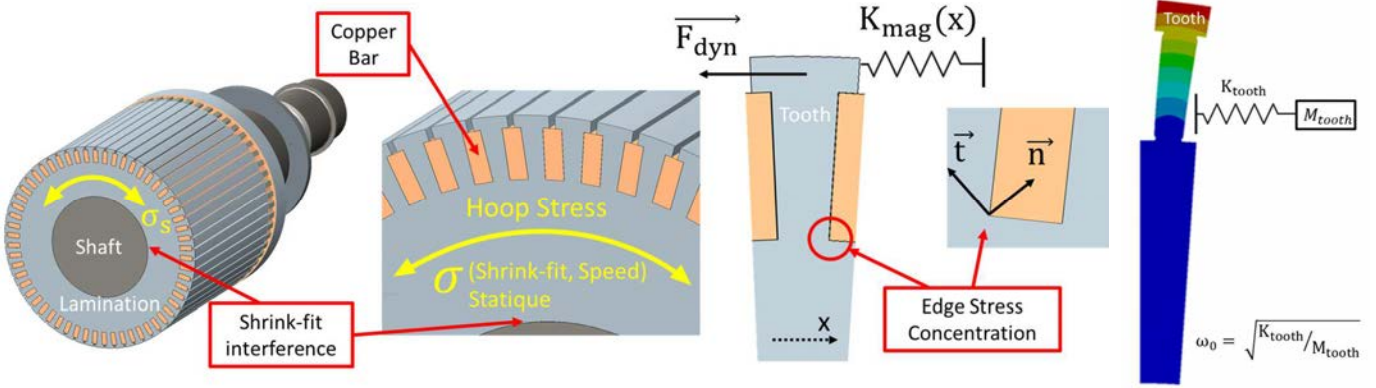

Figure 21 – Overview of Rotor Stresses Model   **Figure 22 – Rotor Tooth Frequency**

The dynamic motion equation is nonlinear, due to the periodic electrodynamic stiffness term $K_{mag}(x)$ induced by the spatial coupling of the stator slots passing frequency seen from the rotor. This equation has the form of a differential equation of Mathieu which, in addition to eigenvalues of rank 1, produces parametric eigenvalues of rank 1/2, 3/2 and 2. The measurements of vibrations on the bearing housings with accelerometers show these bands of parametric excitations (figure 25). For 2-pole motors the parametric coupling being weak, only the coincidences with ranks 1 and 2 are avoided, ranks 0.5 and 1.5 being negligible. Both Finite Element Analysis and bump tests measurement of the teeth natural frequencies are performed (figure 24).

$$M_{tooth}.\frac{d^2x(t)}{dt^2} + C_{tooth}.\frac{d\,x(t)}{dt} + \left(K_{tooth} - K_{mag}(x)\right).x(t) = F(t) \tag{14}$$

$$\frac{d^2x(t)}{dt^2} + 2.\xi.\omega_0\,.\frac{d\,x(t)}{dt} + \omega_0^2\left\{1 - \frac{\kappa.\left(B_n^{(1)}.B_t^{(N_s)} + B_t^{(1)}.B_n^{(N_s)}\right).\,\sin\left(\frac{N_s}{R}.x\right)}{K_{tooth}}\right\}.x(t) = \frac{F_{dyn}(t)}{K_{tooth}} \tag{15}$$

$$\omega_0 = \sqrt{K_{tooth}/M_{tooth}} \tag{16}$$

$$B_n = f\left(\frac{1}{Airgap}\right) \text{ and } B_t = f(Load) \tag{17}$$

The superposition of the static and dynamic principal stresses σ_1 *et* σ_2 makes it possible to model the stress concentration at the surface

of the tooth. An optimized edge shape reduces it. This design is reliable up to 170m/s of rotor peripheral speed, for power around 26MW at 3600 rpm and 8MW at 6000 rpm.

$$[\vec{\sigma}_{tooth\ edge}] = [\vec{\sigma}_{\text{Statique}}] + [\vec{\sigma}_{\text{Dynamique}}] = \begin{bmatrix} \sigma_1 & 0 \\ 0 & \sigma_2 \end{bmatrix} \cdot \begin{Bmatrix} \vec{n} \\ \vec{t} \end{Bmatrix} \tag{18}$$

$$\sigma_1 = 0 \quad \text{and} \quad \sigma_2 = \sigma_{\text{Statique}}(\text{Lamination Shrink\_fitting}, \text{Speed}) + \sigma_{Dynamique}(\text{x(t)}) \tag{19}$$
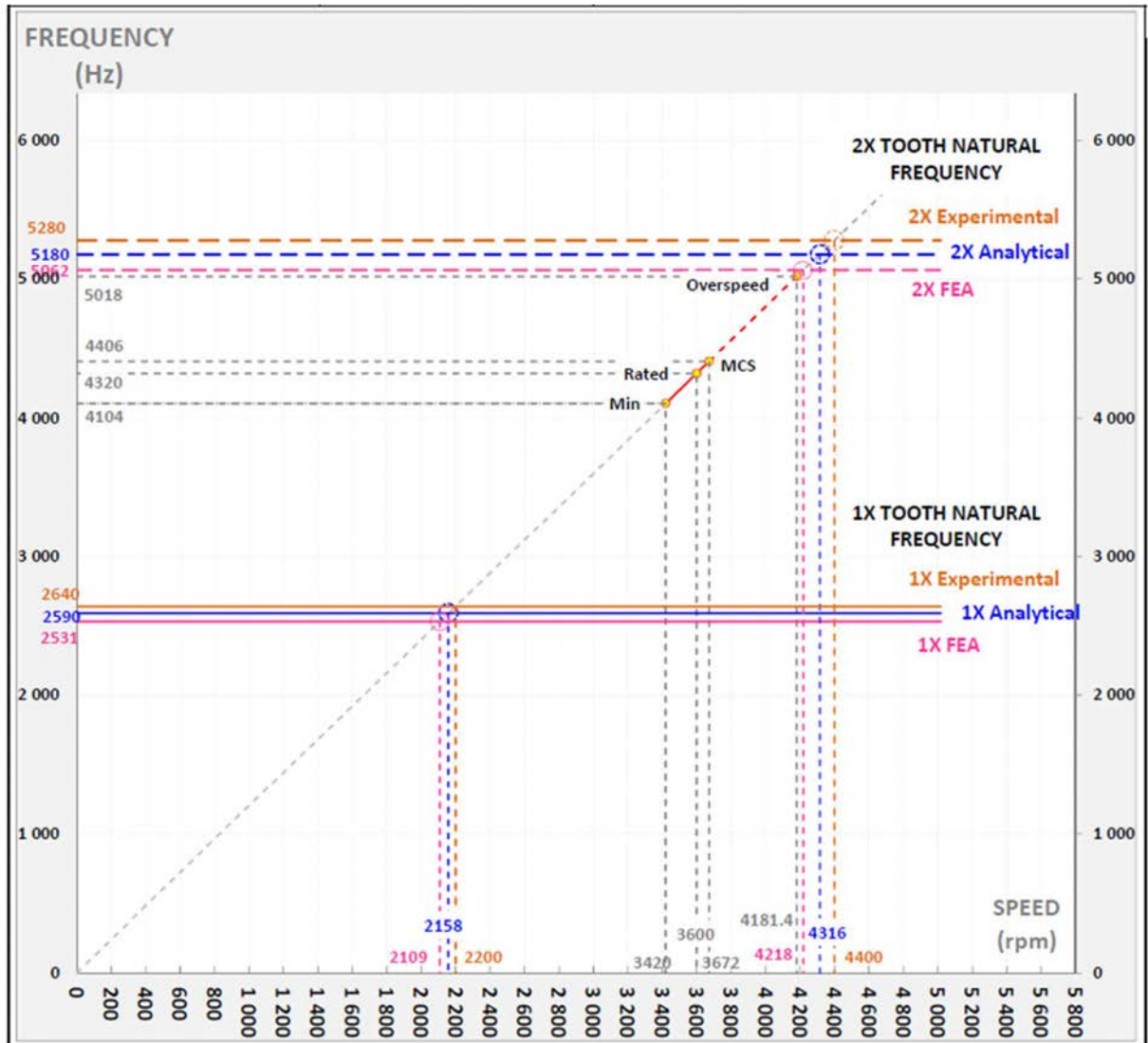
Figure 23 – Rotor Tooth Bending Campbell Diagram
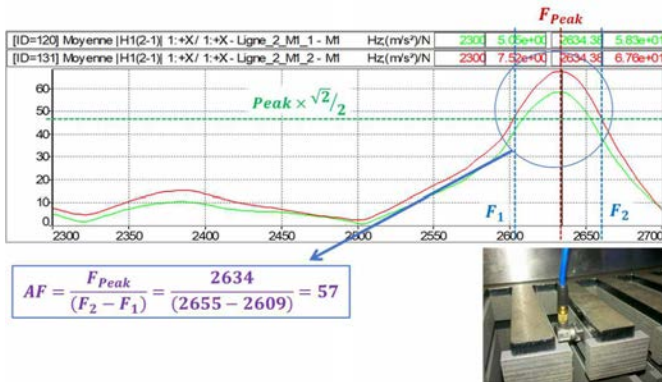
Figure 24 - Rotor Tooth Natural Frequency by Bump Test
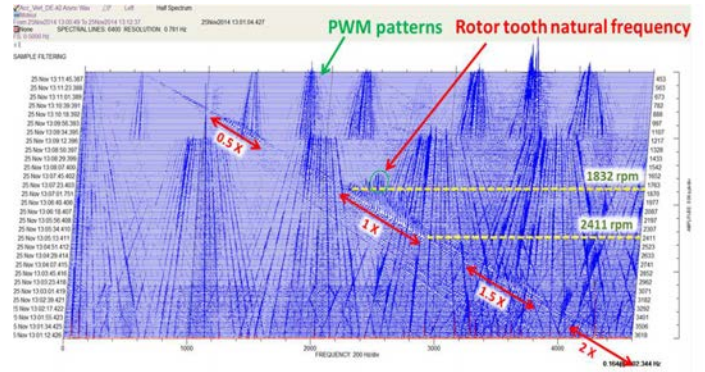
Figure 25 – Vibrations Rotor Tooth Waterfall Diagram

    d.   *Motor Mechanical Integration*

Three mechanical advanced numerical models are also needed for the variable speed motor design considering the speed range interaction against mechanical natural frequencies of the system:

- Rotodynamic Finite Element Analysis to predict motor shaft vibrations,
- 3D Finite Element Analysis (FEA) to predict frame and stator vibrational behavior,
- Full compression train torsional analysis including the electric motor.

The motor is modeled on its foundations for the lateral and structural behavior in different installation scenarios (e.g. FAT, String tests and final site conditions). The finite element rotodynamic model takes account the rotor, the bearings, the motor frame stiffnesses. The site foundations and soleplates used for FAT are modelled as equivalent dynamics stiffnesses (figure 26):

$$K_{ij}^{dyn}(\omega) = K_{ij} - \omega^2 M_{ij} = F_i(\omega) * \frac{\overline{U}_{Re,j}(\omega)}{\overline{U}_{Re,j}^2(\omega) + \overline{U}_{Im,j}^2(\omega)} \tag{20}$$

$$C_{ij}^{dyn}(\omega) = -\frac{F_i(\omega)}{\omega} * \frac{\overline{U}_{Im,j}(\omega)}{\overline{U}_{Re,j}^2(\omega) + \overline{U}_{Im,j}^2(\omega)} \tag{21}$$

where $\overline{U}_{Re}$ and $\overline{U}_{Im}$ are the real and the imaginary complex averaged displacements at the nodes of the interface of fixation and i,j={x,y,z}.

The motor is compliant to API 541 for the shaft displacements, and the bearing and frame vibrations, considering the stiffness and damping matrixes of the 4 lobes bearings at minimum, rated and maximum temperature of oil and the minimum, rated and maximum clearances of the sleeves (figure 27).

Conventional trains present complex torsional behavior. Their equivalent models contain multiple inertias and stiffnesses (motor, low speed coupling, gear wheel, gear pinion, high speed coupling, compressor). The combination with the high motor shaft inertia results in high modal density at low frequency that must be checked carefully. On the contrary, the direct drive starter-helper moto-compression shaft line presents a very simple torsional model, consisting of the motor, compressors and turbine equivalent torsional model, coupled by the couplings stiffnesses. This results in the first 5 torsion modes being less than 47Hz without any risk of excitation in the rotational speed range (figure 28). Again, the VSI induces overall very low torque ripples to the motor and does not produce significant inter-harmonic interactions in between the grid and the motor as for torsional sub-synchronous excitation improving a lot the system reliability. Significant torsional shaft excitations are unlikely to occur.
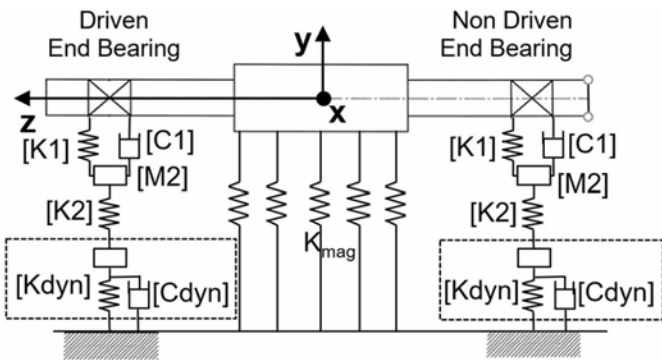
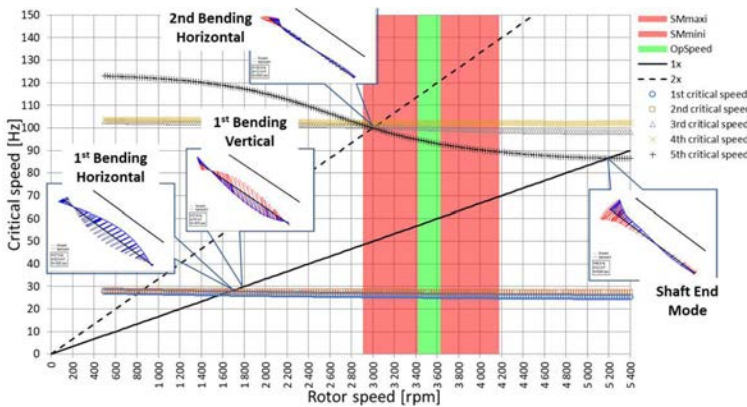**Figure 26 - Rotor Dynamic Model for FEA Lateral Analysis**

Figure 27 -   Lateral Analysis Campbell Diagram @ FAT Conditions
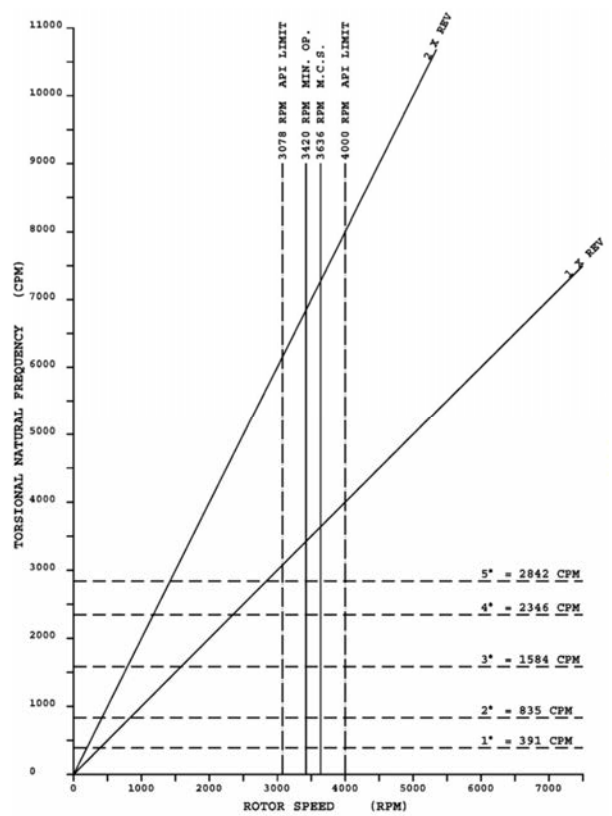

Figure 28 – Torsional Campbell Diagram of Full Train

For structural integration, the full motor, including the rotor with the bearing's symmetric stiffness and damping matrixes, is modelled with a mix 3D/shell FE model predicting the vibrations when the structure is excited by the rotor unbalances and the stator by the pole passing frequency at $2xf_s$ [9] [10].The sensitivity study of foundations shows the needs of stiffness of foundations and motor soleplates above 10^9N/m to avoid any modes of the stator coupled with the frame in the 1X and 2X speed range, especially the horizontal bending mode of the frame (figure 29). The dynamic stiffnesses of the soleplates in vertical, horizontal and axial axis are measured above 5.10^9N/m without any natural frequency from 0 to 200 Hz (figures 31 and 32). During FAT, an Operational Deflection Shape (ODS) of the motor fitted on the soleplates is performed and validate the mode safety margin of the horizontal mode of the frame (figure 30).
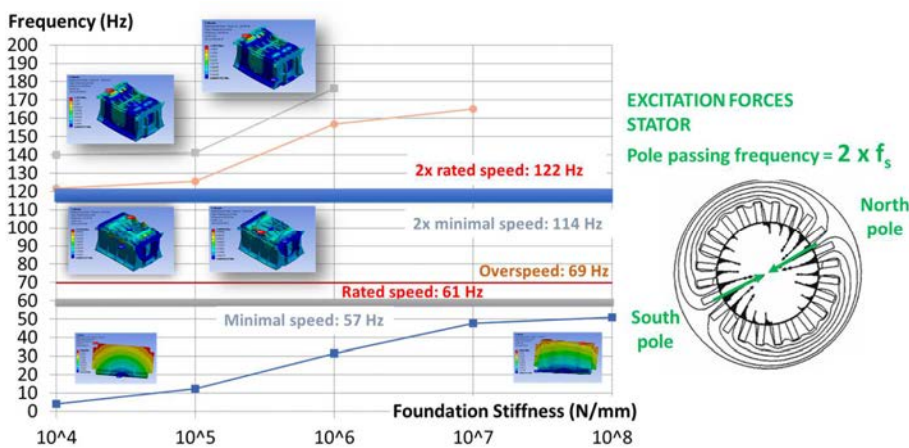

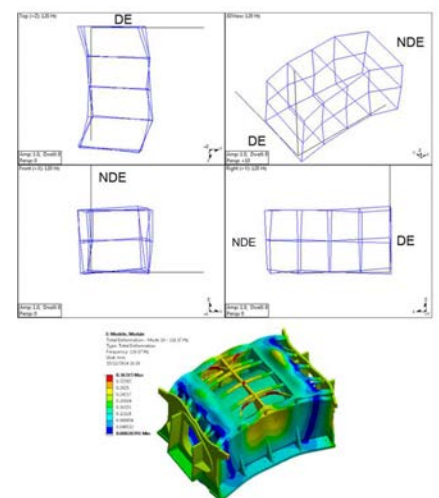**Figure 29 – Motor FEA Sensitivity Analysis vs Foundation Stiffness**

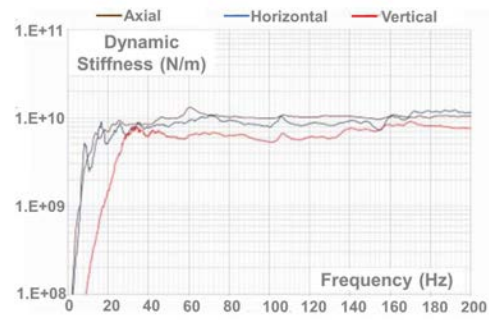**Figure 30 - Motor Horizontal Bending Mode: ODS vs FEA**
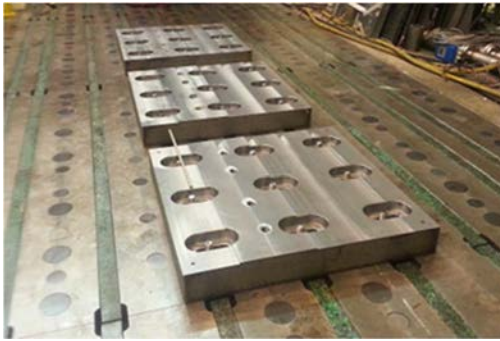
Figure 31 - Motor soleplates for Factory Acceptance Test (FAT)   **Figure 32 – Experimental Dynamic Stiffnesses of Soleplate**

4. TESTS FOR SYSTEM VALIDATION

Validation tests of large LNG trains in full electric configuration or gas turbine with starter helper, require generally a full load combined test of the electrical systems (Motor + Drive + Transformer) in back to back arrangement with a load machine. This kind of test is complex, expensive and time consuming. For systems using an induction machine fed by a VSI converter, the load test is replaced by an alternative heating method and a rotor heating test before carrying out the string tests of the train. Finally, not having to perform combined tests allowed the end-user to save \$1million in project cost as well as a 2-month lead time reduction [11]. After acceptance by the End-user and EPC, the following tests for each system of moto-compression are performed avoiding combined tests:

1. VSDSs and transformers FAT tested at reduced load.
2. Induction rotor overspeed at Rated Speed +20%.
3. Motors FAT at no load, on rigid soleplates (figure 33).
4. Motor Heating Tests for assessing rotor thermal stability and the stator temperature rise.
5. Compressor rotor overspeed at Rated Speed +20%.
6. Compressor FAT.
7. String tests with the full equipped moto-compressor on its skid, the compressor unit control panel, the cables, the VSDS in its shelter, the transformer, and the turbine in case of helper motor configuration (figure 35).

Before final site commissioning, a string test of the full train of compression at full load was carried out in the OEM's test facilities to demonstrate the performance of the complete compressor package under full load conditions, the functionality of the main auxiliary systems and the mechanical behavior of the full shaft line. The main tests outputs of the induction motor are summarized in Table 4.

Figure 33 – Motor during FAT   **Figure 34 – Motor Integrated on Train**   **Figure 35 – String Test Arrangement**

During FTA, the analysis of trends and vibration plots during start up, shut down and steady state conditions reveals a very good mechanical behavior at cold or hot conditions of temperature inside the squirrel cage, with shaft displacements below 20 um p-p in the entire speed range and amplification factor on the first bending modes less than 15 (figures 38 to 43).

The vibrations remain compliant to API 541 (< 38 ump-p) during string tests and in operational conditions on site (figure 44). The motor is initially design at 20MW. It has a temperature margin to operate up to 23MW (figure 37).
The electromagnetic torque produced in the air-gap of the machine, between the stator and the rotor, can be calculated with the

experimental measurement of the stator voltage U(t) and current I(t) of each phase k where k ∈ {1,2,3} using the equivalent phase circuit of the induction machine described as follow:
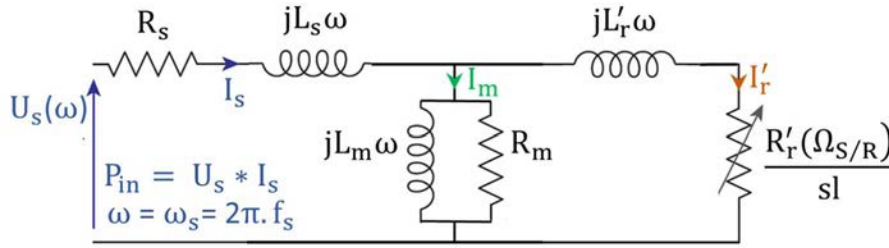

Figure 36 - Induction motor equivalent circuit for one phase

The input power (P_{in}), stator joule losses (P_{Js}), and losses of magnetization (P_m) are respectively given as follow:

$$P_{in} = \sum_{k=1}^{3} U_s^{(k)}(t) . I_s^{(k)}(t) \tag{22}$$

$$P_{Js} = \sum_{k=1}^{3} R_s . I_s^{(k)}(t)^2 \tag{23}$$

$$P_m = \sum_{k=1}^{3} . U_s^{(k)}(t)^2 / R_m \tag{24}$$

The transmitted power is the absorbed power by the electric network from which the losses pertaining to the stator and the magnetization losses are subtracted:

$$P_{TR} = P_{in} - P_{Js} - P_m \tag{25}$$

The power transmitted to the rotor is pulled by the load, plus the Joule losses at the rotor, because the rotor iron losses are negligible knowing that the rotor frequency Ω_{rs} at rated load are very low at a maximum of 3Hz, are negligible. We therefore get:

$$P_{Jr} = sl . P_{TR} \tag{26}$$

The mechanical power (P_{mec}) is the output power to the load:

$$P_{mec} = (1 - sl) . P_{TR} \tag{27}$$

Thus, the electromagnetic torque in the airgap is equal to:

$$\Gamma_{em} = \frac{P_{mec}}{\Omega_r} = \frac{P_{TR}}{\omega_s} \tag{28}$$

The voltage, current and torque curve vs time and spectrum at rated speed are presented in figures 45 to 50, showing the smoothing of the harmonics of current by the sinus filter and the stator inductance. As predicted by calculation, the main torque harmonic contribution is the rank 18 with an amplitude less than 7% of the mean torque.

Table 4 - Main Outputs of the 2-Pole Induction Motor Performance		
Parameters	Acceptance Criteria	Tests Conditions or Results
Rated speed	/	3612 rpm
Motor Power	/	20 MW
Fundamental Motor Voltage	/	9.2 kV
Motor Current	/	1562 A
Winding Temperature at full load	F-Class < 120°C	Max 111.1 °C
Current unbalance	< 2%	Max 1.3%
String Test Radial Vibration on Load	80 um pk-pk	Max 20 um pk-pk
String Test Frame Vibration on Load	3.5 mm/s rms	Max 2.4 mm/s rms
Efficiency @ 100% Load	97%	98.21%
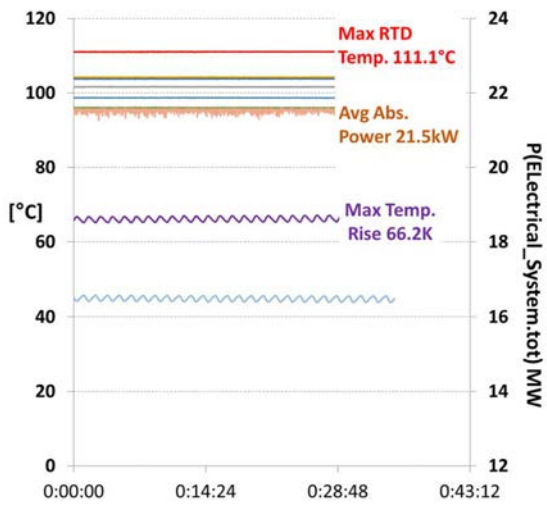
Figure 37 – Temperature Trends during String Tests
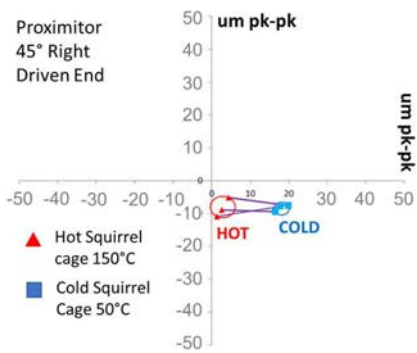

Figure 38 – Driven End (DE) Shaft Displacement at Cold and Hot Temperature of Squirrel Cage
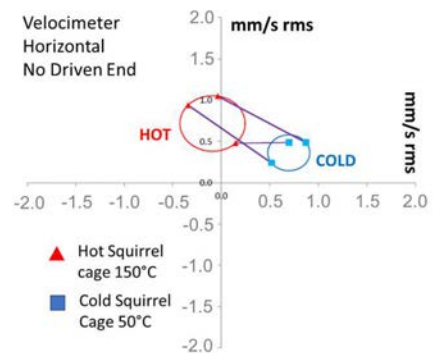

Figure 39 – Non-Driven End (NDE) Bearing Velocity at Cold and Hot Temperature of Squirrel Cage
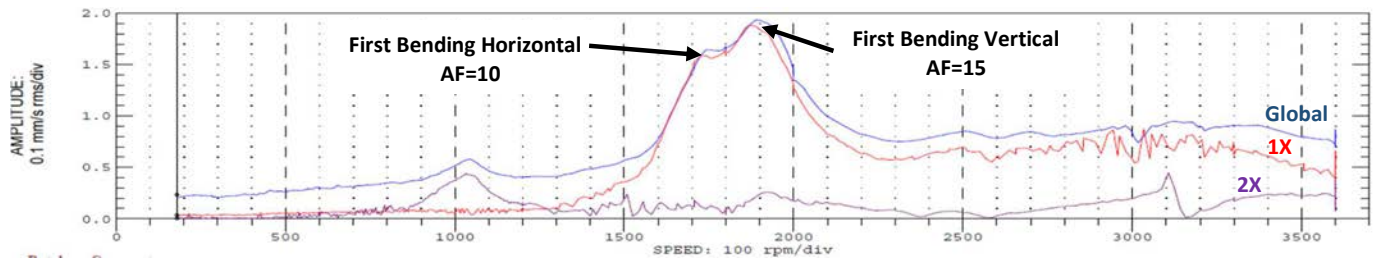
Figure 40 – Vertical DE Motor Bearing Velocity during Ramp Down @ FAT on Soleplates
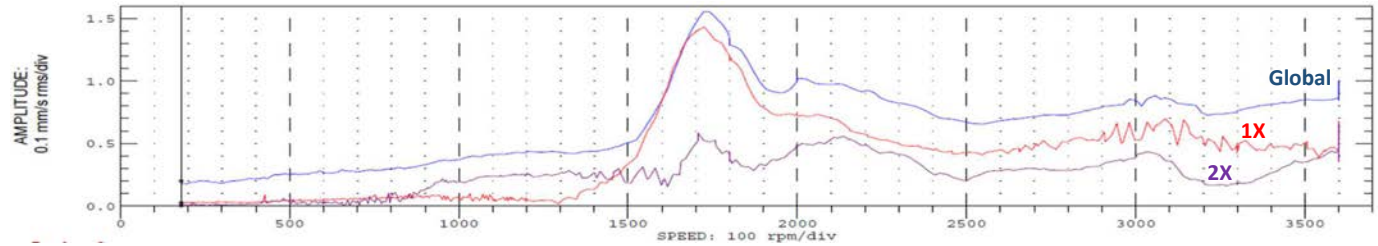

Figure 41 – Horizontal DE Motor Bearing Velocity during Ramp Down@ FAT on Soleplates
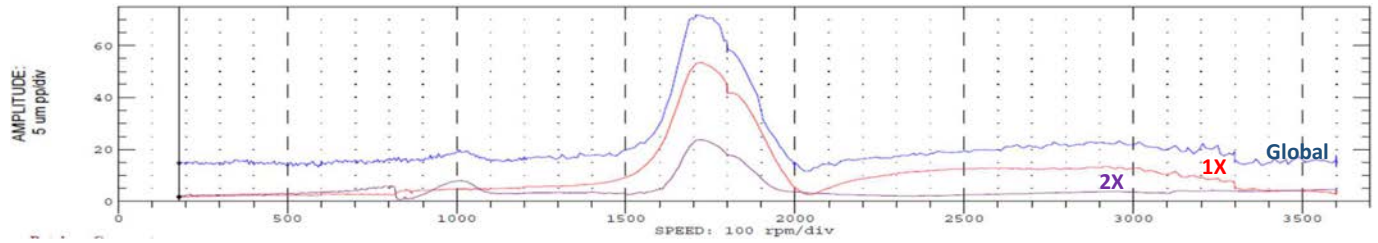

Figure 42 – 45° Left DE Motor Shaft Displacement during Ramp Down@ FAT on Soleplates
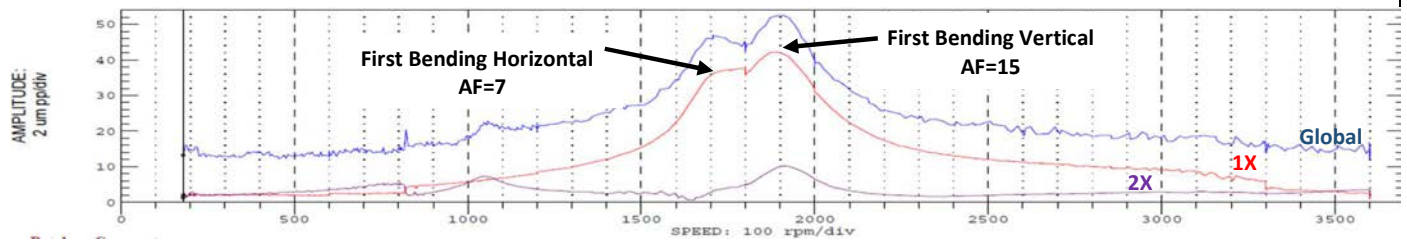

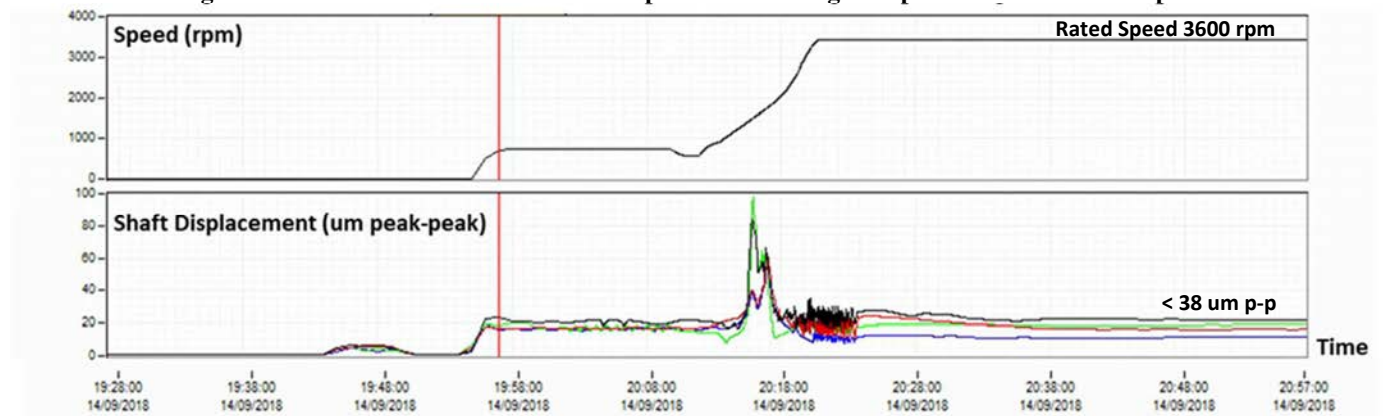**Figure 43 – 45° Left NDE Motor Shaft Displacement during Ramp Down@ FAT on Soleplates**

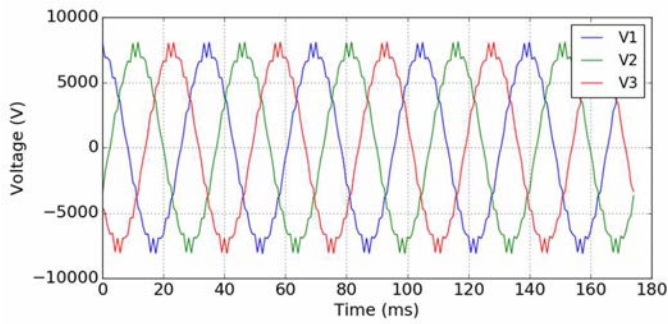
Figure 44 – Shaft Displacements during Ramp Up @ On Site
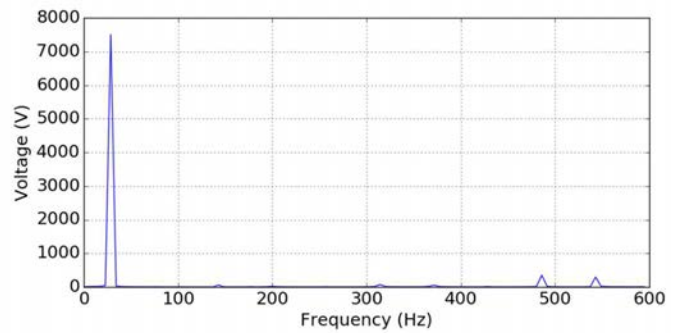
Figure 45 – Stator Voltages (Phase to Ground) vs Time
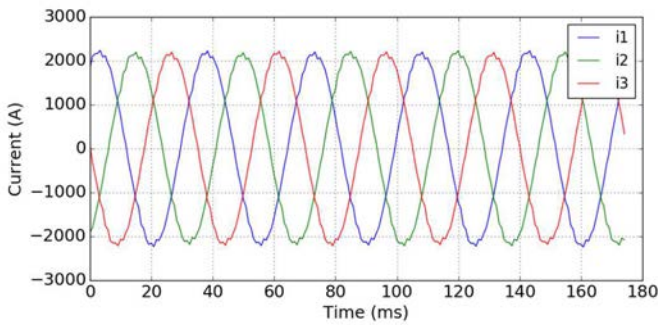

Figure 46 – Stator Voltage (0- Peak) Spectrum
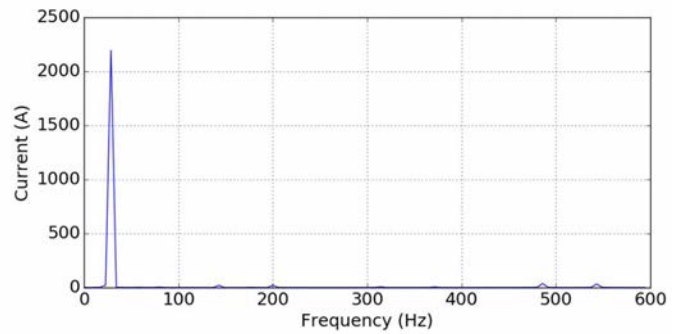

Figure 47 – Stator Currents vs Time

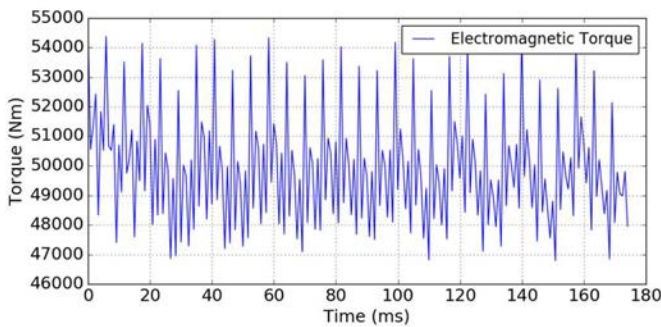**Figure 48 – Stator Current (0- Peak) Spectrum**

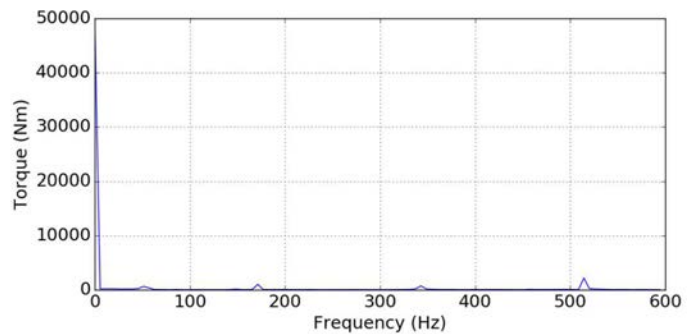**Figure 49 – Air-gap Electromagnetic Torque vs Time**

Figure 50 – Air-gap Electromagnetic Torque Spectrum

CONCLUSIONS AND PERSPECTIVES

This paper presents a comparison between an induction motor powered by VSI and a synchronous motor powered by LCI for the architecture of an 85MW LNG compression train featuring a 20MW VSI motor starter-helper system for a plant in US. It highlights the simplification of the electrical lineup and details the elimination of the large reactive power compensators (capacitors) and of the harmonic filters, the downsizing of the cooling units. The VSI induction motor system is clearly more advantageous in terms of CAPEX and OPEX. The advantages of the induction motor compared to the synchronous motor includes no system of excitation and simplified rotor construction, leading to longer run-time with fewer maintenance issues. Due to the capacitance bank installed on the DC bus of the VSI which kills the low-frequency voltage ripples, there is also no concern about problems of inter-harmonics on the grid and low-frequency torque pulsations interacting with the full LNG train. The electrical system is compliant the IEEE and API requirements and demonstrated a very high level of performance during tests and on site.

To conclude, the full electric compression using the VSI induction motor technology is also available for most LNG and upstream oil and gas applications and is easy to integrate into both public grids and island power generation, especially when equipped with Active Front End (AFE) rectifier technology. The AFE is composed of self-commutated power devices. Usually, its components and its topology are the same as the ones used for the inverter to which it is associated. The AFE is a mirrored image of the inverter (figure 51).

This application is for either helper motor with gas turbine as main driver and it can be also considered also for compressor with motor as main driver (full electric). Above 26MW at 3600 rpm, the technology of rotor construction with the laminated ferromagnetic part hooped on the shaft is not achievable. The technology of shaft-less rotor must be considered (figure 52), achievable up to 120MW (figure 53) [2]. The squirrel cage rotor is adapted for high speed conditions and comprises a steel lamination assembly compressed by tie rods between two end rings and two shaft ends [11].
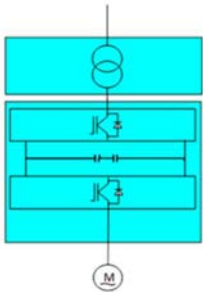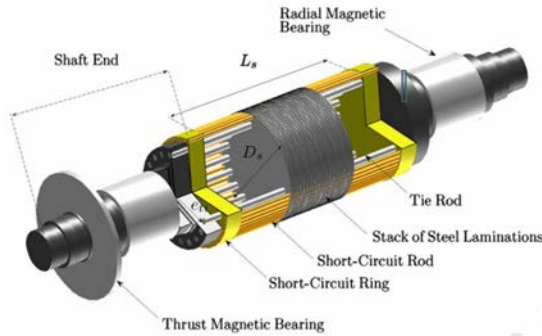

Figure 51 - AFE　　**Figure 52 - Shaftless Laminated Induction Rotor**　　**Figure 53 – 80 MW/4000 rpm Shaftless Induction Rotor**

NOMENCLATURE

A	= Magnetic potential vector	(T.m)
AFE	= Active front end rectifier	
B	= Induction field vector	(T)
B_n	= Normal induction	(T)
$B_n^{(1)}$	= Normal induction of rank 1	(T)
$B_n^{(N_s)}$	= Normal induction of rank N_s	(T)
B_s	= Stator induction field	(T)
B_t	= Tangential induction	(T)
$B_t^{(1)}$	= Tangential induction of rank 1	(T)
$B_t^{(N_s)}$	= Tangential induction of rank N_s	(T)
CAPEX	= Capital expenditure	
C_1	= Oil film damping	(Ns/m)
C_2	= Bearing damping	(Ns/m)
C_{dyn}	= Foundation dynamic damping	(Ns/m)
C_{tooth}	= Rotor tooth damping	(Ns/m)
DE - NDE	= Driven end – No driven end	
DFE	= Diode front end rectifier	
DOL	= Direct on line	
EPC	= Engineering Procurement Construction	
FAT	= Factory acceptance test	
f_g	= Grid frequency	(Hz)
f_s	= Stator frequency	(Hz)
F	= Magnetic force vector	(N)
$F_{dyn(t)}$	= Dynamic force	(N)
F_{pole}	= Magnetic Polar Force	(N)
Γ	= Torque vector	(N.m)
Γ_{em}	= Electromagnetic torque	(N.m)
Γ_h	= Torque harmonic of rank h	(N.m)
Γ_{mean}	= Mean torque	(N.m)
I_h	= Current harmonic of rank h	(A)
I_m	= Magnetization current	(A)
I_r	= Rotor current on rotor referential	(A)
I_r'	= Rotor current on stator referential	(A)

I_s	= Stator current	(A)
IEGT	= Injection enhanced gate transistor	
$\mathbf{J}$	= Current density vector	(A/m²)
$\mathbf{J_s}$	= Stator current density vector	(A/m²)
K_1	= Oil film stiffness	(N/m)
K_2	= Bearing stiffness	(N/m)
K_{dyn}	= Foundation dynamic stiffness	(N/m)
$K_{mag}(x)$	= Magnetic stiffness	(N/m)
K_{tooth}	= Rotor tooth stiffness	(N/m)
κ	= Coefficient	(-)
κ_i	= Coefficient	(-)
l	= Iron length	(m)
L	= Inductance	(H)
L_m	= Magnetization inductance	(H)
L'_r	= Rotor inductance on stator referential	(H)
L_s	= Stator inductance	(H)
LCI	= Load commutated inverter	
MCS	= Maximum continuous speed	
MTBF	= Mean time before failure	
MTTR	= Mean time to repair	
M_{tooth}	= Rotor tooth dynamic mass	(kg)
M_2	= Bearing dynamic mass	(kg)
NPC	= Neutral point clamped	
NPP	= Neutral point piloted	
μ	= Magnetic permeability	(H/m)
N_s	= Stator slot number	(-)
ODS	= Operational deflection shape	
ω_0	= Rotor tooth natural pulsation	(Rad/s)
ω_s	= Stator pulsation	(Rad/s)
Ω_r	= Rotational pulsation	(Rad/s)
Ω_{rs}	= Slippage	(Rad/s)
OEM	= Original Equipment Manufacturer	
OPEX	= Operational expenditure	
p	= Number of pole pair	(-)
P_{in}	= Input power	(W)
P_{Jr}	= Rotor joule losses	(W)
P_{Js}	= Stator Joule losses	(W)
P_{mec}	= Mechanical power	(W)
P_M	= Mechanical losses	(W)
P_{TR}	= Transmitted power	(W)
PWM	= Pulse width modulation	
q	= Electric charge	(C)
R	= Airgap radius	(m)
RAM	= Reliability, availability, maintainability	
R_{Rotor}^{Outer}	= Rotor outer diameter	(m)
R_{Stator}^{inner}	= Stator inner diameter	(m)
R_m	= Magnetization resistance	(Ω)
R'_r	= Rotor resistance on stator referential	(Ω)
R_s	= Stator resistance	(Ω)
ρ	= Electric Resistivity	(Ω/m)
SSTI	= Sub synchronous Torsional Interaction	
$[\sigma_{dynamique}]$	= Dynamic stress tensor	(N/m²)
σ_n	= Normal magnetic pressure	(N/m²)
$[\sigma_{statique}]$	= Static stress tensor	(N/m²)
σ_t	= Tangential magnetic pressure	(N/m²)
$\sigma_1 ; \sigma_2$	= Principal stresses	(N/m²)

sl	= Slip	(-)
$[T_m]$	= Maxwell magnetic tensor	(N/m²)
U_s	= Stator phase to phase voltage	(V)
V_h	= Voltage harmonic of rank h	(A)
VPI	= Vacuum pressure impregnation	
VSI	= Voltage source inverter	
TDD	= Total demand distortion	
ξ	= Damping ratio	(-)

REFERENCES

[1] Pelagotti, A. And Baldassarre, L, Sept-7 2017, ᴀLatest Advances in LNG Compressors - An Overview of New or Updated Technologies at LNG Plants Around the World,@ CompressorTech2 Journal.

[2] Durantay, L., Taillardat, J. M., Pradurat, J. F., and Velly N., 2018, ᴀState of the art for full electric driven refrigeration compressors solutions using adjustable speed drive: which combination of technology leads to the best CAPEX and OPEX solution up to 100 MW,@ IEEE Transactions on Industry Application, *54*, pp. 2992-3004.

[3] Svetti, F., Sgro, D., Rotondo, P. And Meuci, F., Sept 2015, ᴀPractical Guidelines For O&G Plant Design Against Sub-Synchronous Torsional Interaction Phenomena,@ TPS Houston Conference Record.

[4] Yin, W., Durantay, L., Zhang, L., Ul Haq, S. And Vannay F., July 2018, ᴀEnd Winding Protections Improvements Helping to Downsize dV/dt Filter for Medium Voltage Machines Fed by NPP Multi-levels VSI Drive, @ IEEE Budapest International Conference on Dielectrics 2018.

[5] Durantay, L., Karakus, Y., Corentin, L. And Ul Haq, S., Feb 2019, ᴀImprovement of Insulation System for Electrical Rotating Machines up to 15.9kV,@ IEEE PCIC Abu Dhabi Conference Record.

[6] Durantay, L., Alban, T., Siala, S., And Billaud A., Sept 2018, ᴀSelection and Tests of Innovative Variable Speed Motor-Compressor Solutions for a 55MW Full Electric Off-shore Platform Maximizing Availability and Efficiency with Better Environmental Impact,@ IEEE PCIC Cincinnati Conference Record.

[7] Gerada, D. And Brown, N., 2014, ᴀHigh-speed Electrical Machines: Technologies, Trends and Developments, @ IEEE Transactions on Industrial Electronics, *61*, pp. 2946-2959.

[8] Delhaye, G., Velly, N., Quoix, B. And Gelin, A, Sept 2016, ᴀAsynchronous Motor – Failure of Rotor Lamination Teeth,@ TPS Houston Conference Record.

[9] Holopainen, T. P., Roivainen, J. And Aarnivuo S., Sept 2018, ᴀHow to Ensure Low Vibration of 2-Pole Motors on Flexible Foundation,@ IEEE PCIC Cincinnati Conference Record.

[10] Durantay, L., Roth, L., Spolveri N. And Jalabert, S., June 2018, ᴀMain Electro-Mechanical Design and Tests Challenges for Large e-LNG LCI System,@ IEEE PCIC Europe Antwerp Conference Record.

[11] Durantay, L., Clark, T., Roth, L. And Galmiche C., Sept 2019, ᴀAlternative Package of Tests to Reduce CAPEX and Delivery Time of Large LNG Train Using Induction Machine Fed by VSI Drive Technology Up to 120MW,@ IEEE PCIC Vancouver Conference Record.

ACKNOWLEDGEMENTS